Double Electron Electron Resonance as a Method for Characterization of Micelles

Sharon Ruthstein,[†] Alexey Potapov,[†] Arnold M. Raitsimring,[‡] and Daniella Goldfarb*[,†]

Department of Chemical Physics, Weizmann Institute of Science, Rehovot, 76100, Israel, and Department of Chemistry, University of Arizona, Tucson, Arizona 85721

Received: August 9, 2005; In Final Form: September 24, 2005

Double electron electron resonance (DEER) is an experimental technique used to determine distance between electron spins. In this work, we show that it can be used to study the properties of micelles in solution, specifically their volume and the aggregation number. The feasibility of the method is tested on micelles of Pluronic block copolymers, $PEO_x-PPO_y-PEO_x$, built from chains of poly(ethylene oxide) (PEO), comprising the more hydrophilic corona, and a poly(propylene oxide) (PPO) block constituting the hydrophobic core. In this work, the dimensions of the hydrophobic core of micelles of Pluronic L64 ($x = 13$, $y = 30$), P123 ($x = 20$, $y = 70$), and F127 ($x = 106$, $y = 70$) and their aggregation number were studied. This was done using the spin-probe 4-hydroxy-tempo-benzoate (4HTB), which is hydrophobic and is localized in the hydrophobic core of the micelles and does not dissolve in aqueous solution. The measurements were carried out on frozen solutions, freeze quenched after equilibration at 50 °C. It was found that the hydrophobic core radii occupied by 4HTB in 7.5 wt % F127 and 6 wt % L64 are 4.0 ± 0.05 and 3.8 ± 0.1 nm, respectively, and the corresponding aggregation numbers are 57 ± 2 and 206 ± 14. The micelles of 6 wt % P123 were found to have a rod shape, and the addition of 4HTB at concentrations higher than 0.7 mM resulted in a phase transitioned to spherical micelles. Finally, this study also showed that the micelle structure is preserved upon rapid freezing.

Introduction

Water-soluble triblock copolymers of poly(ethylene oxide) (PEO) and poly(propylene oxide) (PPO), often denoted $PEO_x-PPO_y-PEO_x$, are commercially available, nonionic, macromolecular surface active agents.[1,2] Variation of the copolymer composition (PPO_y/PEO_x ratio) and molecular weight (PEO_x and PPO_y block length) allows the production of molecules with optimized properties that meet the specific requirements in various areas of technological significance. As a result, $PEO_x-PPO_y-PEO_x$ block copolymers comprise an important class of surfactants and find widespread industrial applications in detergency, dispersion stabilization, foaming, emulsification, lubrication, and formulation of cosmetics.[2] The commercial names for these surfactants are Poloxamers (manufactured by ICI) and Pluronic (manufactured by BASF). A recent, interesting, and important application of Pluronics is their use as templates in the synthesis of highly ordered mesoporous materials.[3,4] There, the starting materials consist of a dilute solution of Pluronic micelles, which upon the addition of a silica precursor such as an organosilane or sodium silicate, in acidic media, yields mesostructures with a variety of hexagonal, lamellar, and cubic structures.[3,5] The removal of the encapsulated Pluronic then produces the high surface area mesoporous material. Hence, understanding the properties of the Pluronic micelles and their transformation is important for rationalizing the formation of these materials.

In comparison to normal surfactants, Pluronics have the peculiarity that their critical micelle concentration (CMC) and their surface activity depend strongly on temperature. The CMCs of the block copolymers can vary by several orders of magnitude within a small temperature range. The main change occurs in the temperature region between 20 and 50 °C. The consequence of this is that in moderately concentrated solutions with 1 wt % polymer, the block copolymers are present in a monomeric state below room temperature and are transformed into micelles at higher temperatures. Usually, the transformations occur over a range of 20 °C.[1,2] For example, Su et al.[6] found by FTIR that the critical micelle temperature (CMT) of a 15 wt % aqueous Pluronic F127 ($PEO_{106}PPO_{70}PEO_{106}$) solution is 17 °C. Above the CMT, there is an equilibrium region, in a temperature range between 17 and 29 °C, referred to as the unimer-to-micelle transition region.

Micellar solutions of block copolymers were investigated with many different techniques including NMR,[7−9] static and dynamic light and neutron scattering,[10,11] fluorescence spectroscopy, and small-angle X-ray spectroscopy (SAXS).[2,12] It was concluded from these measurements that micelles are built from a core consisting of the PPO block and a corona which contains the PEO blocks. The micellization process is strongly driven by entropy, and the free energy of micellization is mainly a function of the PPO block, the hydrophobic part of the polymer.[2] In addition, small-angle neutron scattering (SANS) measurements have shown that for PEO contents larger than 40% (e.g., F127, L64 ($PEO_{13}PPO_{30}PEO_{13}$)) only spherical micelles are present and the transition to rodlike micelles occurs at very high temperatures, $T > 90$ °C.[13] For a moderate content of EO (~30%, e.g., P123 ($PEO_{20}PPO_{70}PEO_{20}$)), rod-shaped micelles may form at lower temperatures.[14] The size of the micelles is usually determined by neutron and light scattering, which provide the hydrodynamic radius of the micelle,[1] namely, an upper limit for the real micelle radius.

* To whom correspondence should be addressed. E-mail: daniella.goldfarb@weizmann.ac.il.
[†] Weizmann Institute of Science.
[‡] University of Arizona.

10.1021/jp054450v CCC: $30.25
Published on Web 11/10/2005

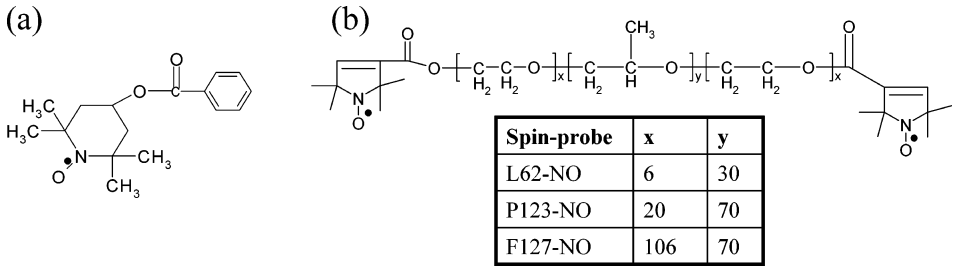

Spin-probe	x	y
L62-NO	6	30
P123-NO	20	70
F127-NO	106	70

Figure 1. Structure of (a) 4HTB and (b) Pluronic spin-probes.

In this study, we introduce a new approach for determining the size of micelles and the aggregation number based on double electron resonance spectroscopy (DEER) which is designed for distance measurements. So far the spin-probe EPR methodology was found to be most useful in the study of the motional characteristics within the micelles based on line shape analysis, for the detection of the unimer−micelle transition and for the evaluation of the polarity profile within micelles.[15−17] Indirect information regarding the micellar size could be obtained from the determination of the correlation time and its analysis in terms of the Debye−Stokes−Einstein equation.[18,19] Here, we take advantage of the recent advances in the DEER technique[20] to determine the local concentration of spin-probes in the micelle, which in turn yields the volume of the micelle. It has already been shown that DEER experiments are excellent for the determination of the distribution of paramagnetic centers in various systems, for example, the structure of double-labeled peptides in aggregates was studied by Milov et al.[21−23] and the size of ion clusters and the distance between them were examined by Pannier et al.[24]

We chose to concentrate on Pluronic P123 which is used as a template for the preparation of the hexagonal mesoporous material SBA-15 and on F127, used for the cubic SBA-16 material. As an additional reference for a relatively short Pluronic we chose L64, which is also used as a template for mesoporous materials.[3] The four-pulse DEER experiment[25] was employed, and the spin-probe used was 4-hydroxy-tempo-benzoate (4HTB). It is hydrophobic and water insoluble and is therefore localized in the hydrophobic core of the micelles. For each micellar solution, the volume of the core and the aggregation number were determined.

Experimental Section

Sample Preparation. The Pluronic block-coplymer

Pluronic P123 (PEO_{20}−PPO_{70}−PEO_{20}), Pluronic L64 (PEO_{13}−PPO_{30}−PEO_{13}), and Pluronic F127 (PEO_{106}−PPO_{70}−PEO_{106}) were a gift from BASF Corp. (USA). The spin-probe 4-hydroxy-tempo-benzoate (4HTB) was purchased from Aldrich. The spin-probes L62-NO, P123−NO, and F127−NO were synthesized as described in the literature.[26] Figure 1 shows the structure of the spin-probes.

4HTB was dissolved in a micellar solution at 50 °C; after stirring for approximately 1 h, a sample from the solution was placed in a 3 mm o.d. Teflon tube and was kept at 50 °C in a hot water bath for 20 min. Then the sample was frozen rapidly by placing the tube in a 2-methyl butane bath cooled by liquid nitrogen.

Spectroscopic Measurements. Continuous wave (CW) EPR spectra were recorded on a Varian E-12 spectrometer operating at a frequency of 9−9.5 GHz. Liquid samples were measured in flat cells. Constant-time DEER measurements were carried out at X-band frequencies with a Bruker Elexsys E 580 spectrometer using the constant-time four-pulse DEER experiment $\pi/2(\nu_{obs}) - \tau_1 - \pi(\nu_{obs}) - t' - \pi(\nu_{pump}) - (\tau_1 + \tau_2 - t') - \pi(\nu_{obs}) - \tau_2 -$ echo.[25] A two-step phase cycle was employed on the first pulse, and an average of over 25 increments of τ_1 ($\tau_1 = 200$ ns, $\Delta\tau_1 = 8$ ns) was carried out to suppress proton modulations.[27] The echo was measured as a function of t', while τ_2 was kept constant at 1.5 μs to eliminate relaxation effects. The pump frequency, ν_{pump}, was set to the maximum of the nitroxide spectrum, and the observer frequency, ν_{obs}, was 60 MHz higher. Both the $\pi/2$ and π pulses had a length of 40 ns, and the dwell time was 20 ns. Typical numbers of shots per point and scans were 30 and 300, respectively, and the measurement temperature was $T = 15$ K.

Theoretical Background. In spin−echo based experiments, the evolution of the spin−echo signal for a single pair (i, k) of dipolar interacting spins is[28]

$$V(t) = V_0[1 - \lambda_k(1 - \cos(\omega_{ik}t))] \tag{1}$$

where t is the appropriate variable time interval, which depends on the chosen technique, and λ_k is the probability to flip one of the two spins by the appropriate pulse, and its average is given by

$$\langle\lambda_k\rangle_{g(\Delta\omega_k)} = \int_{-\infty}^{\infty} \frac{{\omega_1}^2}{{\omega_1}^2 + \Delta{\omega_k}^2} \sin^2\frac{({\omega_1}^2 + \Delta{\omega_k}^2)^{1/2}t_p}{2} g(\Delta\omega_k)\, d\Delta\omega_k \tag{2}$$

where ω_1 and t_p are the amplitude and duration of the π pulse, respectively, $\Delta\omega_k$ is the off-resonance frequency, and $g(\Delta\omega_k)$ is the distribution of $\Delta\omega_k$ which is given by the EPR spectrum. In eq 1, ω_{ik} is

$$\omega_{ik} = \omega_{dd}^{(ik)}(3\cos^2\theta_{ik} - 1) \tag{3}$$

where $\omega_{dd}^{(ik)}$ is the so-called dipolar evolution frequency given by

$$\omega_{dd}^{(ik)} = \frac{\mu_0}{4\pi\hbar}\frac{g_i g_k \mu_B^2}{r_{ik}^3} \tag{4}$$

Spin i is treated as an observer spin (A spin) and spin k as the pumped spin (B spin), g_i and g_k are the electron g values of the two spins, and θ_{ik} is the angle between $\vec{B}_0$ and the vector connecting the loci of the two spins. Henceforth, we assume $g_i = g_k = g$ for all i and k. In a multispin system (many B spins), the echo intensity due to any A spin is thus given by

$$V_i(t) = V_0 \prod_{k\neq i} [1 - \lambda_k(1 - \cos(\omega_{ik}t))] \tag{5}$$

and the total echo is the sum of the echoes from all A spins.

This yields for N interacting spins

$$V(t) = V_0 \langle \prod_{k \neq i}^{N-1} (1 - \lambda_k(1 - \cos \omega_{ik} t)) \rangle \quad (6)$$

where the brackets denote the relevant averaging.

For an isotropic disordered system with a homogeneous distribution of spins, the dipolar time evolution exhibits a monoexponential decay, which depends on the spin concentration, C, according to[29,30]

$$V(t) = V_0 \exp(-t/T_{\text{hom}}) \quad (7)$$

and the time constant, T_{hom}, is

$$T_{\text{hom}} = \frac{9\sqrt{3}\hbar}{2\pi g^2 \mu_B{}^2 \mu_0 \lambda C} \quad (8)$$

Here, λ is the fraction of the excited B spins, given by eq 2. For spin 1/2

$$T_{\text{hom}} = 1.0027 \frac{10^{-3}}{C\lambda} \quad (9)$$

where C is given in moles and T_{hom} in microseconds.

In a system which consists of aggregates, where the average interaggregate distance is larger than the average distance within the aggregate, the DEER decay is often presented as the following product:[21,22,31,32]

$$V(t) = V_{\text{intra}}(t) V_{\text{inter}}(t) \quad (10)$$

where $V_{\text{intra}}(t)$ presents the decay due to spins in the same aggregate, and $V_{\text{inter}}(t)$ is due to the interaction with spins in different aggregates. The determination of $V_{\text{inter}}(t)$ is a complicated problem and was explicitly investigated only in a few publications.[30−33] The case that is most relevant to our investigation is that of polymers sparsely labeled with radicals, which produced "clusters" of radicals with a radical content of 30−45 per cluster and a cluster size of ∼10 nm.[31] On the basis of the data shown in this work, for t values up to ∼2 μs, $V_{\text{inter}}(t)$ can be approximated as[31]

$$V_{\text{inter}}(t) = V_0 \exp(-t/\chi T_{\text{hom}}) \quad (11)$$

where T_{hom} is given by eq 9. This is equivalent to the use of an effective concentration $C_{\text{inter}} = C/\chi$ (C is the average radical concentration) to describe the inter-cluster decay. χ is a parameter which depends on the size of the cluster and, probably, on the amount of radicals in a cluster. For the objects investigated in the work of Milov and co-workers,[31] it can be evaluated to be ∼10, which means that the decay due to inter-cluster dipolar interactions is considerably less than expected for a homogeneous radical distribution in solution. Therefore, despite uncertainty in the evaluation of $V_{\text{inter}}(t)$, we can safely expect that in our case the echo decay caused by inter-aggregate interactions will always be less than that expected for homogeneous radical distribution in solution. Moreover, as the average concentration of the spins increases, this contribution should decrease even further.

For a micellar solution with M_{av} average spins per micelle, $V_{\text{intra}}(t)$ (eq 6) is

$$V_{\text{intra}}(t) = \sum_{M=1}^{\infty} P(M, M_{\text{av}}) \langle \prod_{k \neq i}^{M-1} (1 - \lambda_k(1 - \cos \omega_{ik} t)) \rangle \quad (12)$$

Here, the averaging is over all possible distances within the micelle and all possible orientations with respect to the magnetic field, and $P(M, M_{\text{av}})$ is the Poisson distribution probability. Because there is no correlation between the electron spin positions, the integration can be carried out independently for each spin,[20,33] yielding for the normalized echo intensity

$$V_{\text{intra}}(t) = \frac{1}{2\upsilon} \sum_{M=1}^{\infty} P(M, M_{\text{av}}) [\int_0^{\pi} \int_{r_{\min}}^{r_{\max}} (1 - \lambda(1 - \cos \omega_{ik} t)) r^2 \, dr \sin\theta \, d\theta]^{M-1}$$

$$= \sum_{M=1}^{\infty} P(M, M_{\text{av}}) \Bigg[1 - \lambda + \frac{\lambda}{2\upsilon} \int_0^{\pi} \int_{r_{\min}}^{r_{\max}} (\cos \omega_{ik} t) r^2 \, dr \sin\theta \, d\theta \Bigg]^{M-1} \quad (13)$$

where υ is the volume normalizing factor. In the above, $r_{\max}$ represents the maximum distance between spins and $r_{\min}$ their minimum approach; in the case of spherical micelles, $r_{\max}$ is the diameter of the micelles. For long times, the cos integral averages to zero and

$$V_{\text{intra}}(t) \sim \sum_{M=1}^{\infty} P(M, M_{\text{av}}) [1 - \lambda]^{M-1} \quad (14)$$

using eqs 10, 11 and 14 we obtain

$$V(t) \sim V_0 \exp(-t/\chi T_{\text{hom}}) \sum_{M=1}^{\infty} P(M, M_{\text{av}})) [1 - \lambda]^{M-1} \quad (15)$$

For a long t and small λ values, this further simplifies to[23]

$$V(t) \sim V_0 \exp(-t/\chi T_{\text{hom}}) [1 - (M_{\text{av}} - 1)\lambda] \quad (16)$$

Due to the relatively small number of spins in a micelle and the finite micelle size (with respect to the dipole−dipole interaction range), V_{intra} cannot be approximated as a decay of a homogeneous solution.

For rod-shaped micelles, the distance between the spins, r_{ik}, can be expressed in terms of its lateral component ρ (in the xy plane) and axial component, l, such that $r_{ik} = (l_{ik}^2 + \rho_{ik}^2)^{1/2}$. In this case

$$V_{\text{intra}}(t) = \frac{1}{2\upsilon} \sum_{M=1}^{\infty} P(M, M_{\text{av}}) [\int_0^{\pi} \int_{l_{\min}}^{l_{\max}} \int_{\rho_{\min}}^{\rho_{\max}} (1 - \lambda(1 - \cos \omega_{ik} t)) \rho \, d\rho \, dl \sin\theta \, d\theta]^{M-1} \quad (17)$$

Results

CW EPR Measurements. Initially, CW EPR measurements were carried out to verify that the samples were freeze quenched from a temperature above the CMC. Figure 2a shows the CW EPR spectra of 1 mM 4HTB in an aqueous solution of 3, 4, 5, and 7.5 wt % F127 at 50 °C. The spectrum of the 3 wt % F127 is a superposition of two spectra showing that 4HTB is distributed between two different environments, I and II. Fitting the high field component of the triplet to two Lorentzian lines (the dashed line in the spectrum of 3 wt % F127) showed that the two species have different line widths (Δlw = 2.2 G) and also

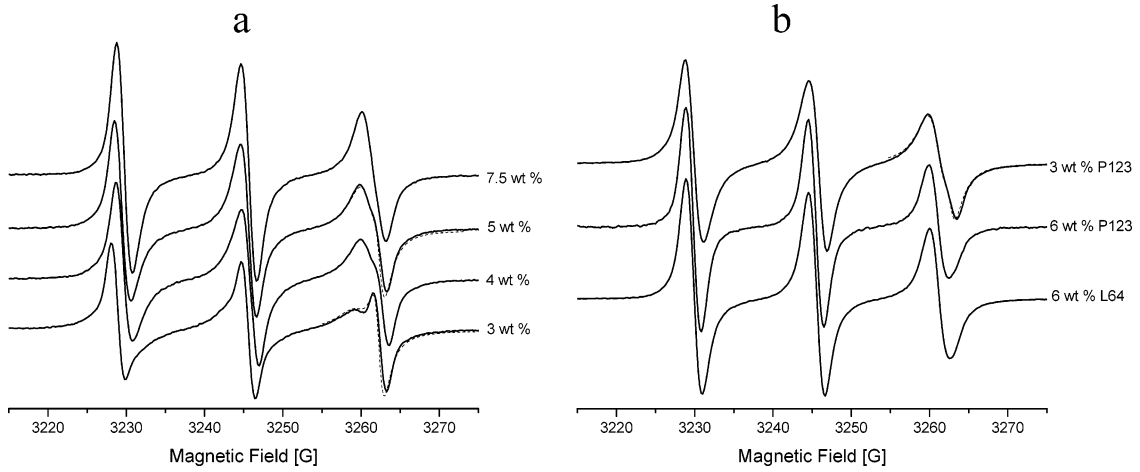

Figure 2. CW EPR spectra at 50 °C of 1 mM 4HTB in (a) an aqueous solution of Pluronic F127 at various concentrations and (b) in aqueous solution of 3 wt % P123, 6 wt % P123, and 6 wt % L64. The dashed lines are the simulated spectra (see text).

a different hyperfine coupling ($a_{N,I} = 17.6$ G, $a_{N,II} = 15.9$ G). The variation in a_N is attributed to a difference in the polarity of the environment, whereas the increase in the line width can be either due to the slower reorientation of the spin-probe or due to a higher local density of spins, which raises the Heisenberg-exchange interaction. The species with the lower a_N value, referred to as I, senses a more hydrophobic environment and has a larger line width. As the concentration of F127 increases, the relative amount of this species increases, and at 7.5 wt %, it becomes the only species present. The spectral deconvolution showed that, at 3 wt % and 5 wt % F127, 49.3% and 68.8%, respectively, of the 4HTB belong to species I.

The 50 °C CW EPR spectra of spin-labeled Pluronics, L62−NO and P123−NO, in 3 wt % F127 also showed the presence of two environments (not shown). F127−NO in the same solution revealed only one species that exhibits a small decrease in a_N ($\Delta a_N = 0.05$ G) at the CMT. This is in contrast to P123−NO, where the difference in a_N at the CMT is 0.7 G and the signals of the two species attributed to unimers and micelles are resolved. In F127−NO, the position of the spin-label is close to the outer edge of the corona, thus making the spectral differences between micelles and unimers very small and within the line width. Hence, for this solution, environment II is attributed to 4HTB solvated in unimers.

Figure 2b compares the spectra of 1 mM 4HTB in 3 wt % P123, 6 wt % P123, and 6 wt % L64 solutions at 50 °C. In 3 wt % P123, 4HTB is again distributed between two different environments with $a_{N,I} = 17.1$ G, $a_{N,II} = 15.5$ G, and $\Delta lw = 1.2$ G, where 82% of the 4HTB probes are in the hydrophobic environment I. At 6 wt % P123 and 6 wt % L64, all the 4HTB probes are in region I, with $a_N = 15.5$ G. The a_N value of 4HTB in 7.5 wt % F127 is somewhat larger, hence it senses a slightly higher polar environment.

An intuitive assignment of the two environments in P123 would be the micelles as the hydrophobic one and the unimers in which the 4HTB is solvated. However, earlier measurements carried out using L62−NO and P123−NO showed that in 3 wt % of P123 at 50 °C all the spin-labeled Pluronic molecules experience only one environment.[34,35] Moreover, the transition unimer−micelles has been detected for these concentrations at a temperature lower than 50 °C based on a change in a_N. Accordingly, we attribute the two environments to micelles where environment II corresponds to 4HTB molecules residing in or close to the corona region. The latter being a less preferred site. As the concentration of the Pluronics increases (while the concentration of 4HTB remains constant), the total hydrophobic volume in the sample increases, causing the migration of 4HTB molecules from the unfavorable corona to the hydrophobic core.

DEER Measurements. The DEER measurements were carried out on a micellar solution freeze quenched after equilibration at 50 °C by dropping it into a 2-methyl butane bath cooled by liquid nitrogen. To test the reproducibility of the freezing procedure, measurements were repeated approximately three times, freezing different samples taken from the same stock solution. The results were highly reproducible. In addition, comparison with the DEER measurements carried out on the same solutions frozen just by liquid nitrogen showed that freezing in 2-methyl butane cooled by liquid nitrogen gave better reproducibility. While the freeze-quench procedure used is fast enough to prevent significant redistribution of the P123 macromolecules between micelles, it is most probably not fast enough to completely prevent conformational changes that are much faster.

F127 and L64. The spin flip probability λ can be easily evaluated from eq 2, by averaging over the distribution of resonance frequencies, which is given by the CW EPR spectrum. However, due to the inhomogeneity of B_1 in the resonator, the real value of λ may be lower than that evaluated through eq 2. To overcome this problem, we extracted this parameter from experimental data obtained for a frozen glassy solution of 4HTB in toluene. The top trace in Figure 3 shows the four-pulse DEER trace of 1 mM 4HTB in toluene, and the corresponding dotted line represents the best fit to a single-exponential decay (eq 7) from which $T_{hom} = 5$ μs was determined. Figure 4 shows that the dependence of T_{hom} on [4HTB] is linear as expected. From the slope, $a = (0.185 \pm 0.01) \times 10^{-3}$ ns^{-1} and eq 9, $\lambda = 0.18$ was evaluated. This value of λ is in a reasonable agreement with the value of 0.21 obtained from eq 2. Figure 3 also shows the DEER experiment for 1 mM 4HTB in 7.5 wt % F127 aqueous solution. The decay of the F127 solution is faster than that in the toluene solution due to the confined volume offered by the micelles. In this case, the data analysis should be done according to eq 13.

To verify whether the DEER decays of the micellar solutions can be analyzed using the long time approximation (eq 15), a number of simulations were carried out using eq 13 for several values of average spins per micelles (M_{av}). The parameters chosen were $\lambda = 0.18$, $r_{min} = 0.3$ nm, and $r_{max} = 10$ nm, which are within the range expected for our samples. Figure 5 clearly shows that at long periods of time the signal reaches a plateau. The value of r_{max} determines the time it takes to reach the plateau, the larger the r_{max} value, the longer the time. For the

TABLE 1: Values of the Diameter (r_{max}) of the Spherical/Cylindrical Volume and the Length (l_{max}) of the Cylindrical Volume that 4HTB Occupies, the Micelles Concentration (C_m), the Aggregation Number (N_{agg}), the Hydrophobic Core Diameter (d_c), and the r_{max}/d_c Ratio, Obtained from Numerical Fitting of the DEER Decays for the Various Pluronic Solutions Studied

	r_{max} (nm)	l_{max} (nm)	C_m (mM)	N_{agg}	d_c (nm)	r_{max}/d_c
3 wt % P123	7.1−7.5		0.091−0.103	52−60	8.7−9.1	0.82
6 wt % P123 (≤0.7 mM), spheres	7.9−8.1		0.084−0.095	114−128	11.3−11.7	0.68−0.7
6 wt % P123 (>0.7 mM), spheres[a]	12.5−12.8		0.104−0.116	93−104		
3 wt % F127[b]	6.5 ± 0.1		0.142 ± 0.006	13−17	5.2−5.7	1.1−1.3
7.5 wt % F127	7.9−8.1		0.104−0.11	55−59	8.8−9.1	0.88−0.9
6 wt % L64	7.5−7.8		0.098−0.11	192−220	10.2−10.6	0.74
6 wt % P123[c] (≤0.7 mM), rods	6.9−7.1	10	0.065−0.068	159−165	11.6−11.8	0.6
6 wt % P123[c] (>0.7 mM), rods	4.9−5.1	20	0.166−0.257	42−64	4.2−5.2	0.96−1.2

[a] In this case, d_c was not calculated because of the effect of 4HTB. [b] In this case, the range is obtained only by taking $C_m M_{av} = C_{inter}$. [c] d_c was calculated, assuming that the hydrophobic core volume $V_m = \pi(d_c/2)^2 l_{max}$.

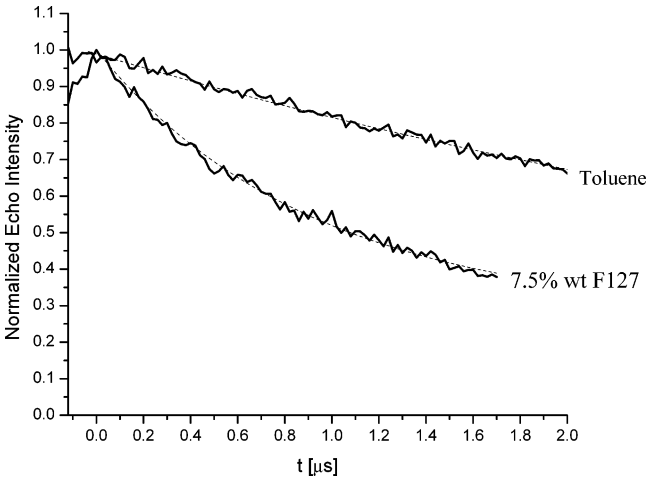

Figure 3. DEER decay of 1 mM 4HTB in toluene and in 7.5 wt % F127. The dashed lines are a first-order exponential decay fit for 4HTB in toluene and a best fit decay for 7.5 wt % F127, obtained with the parameters given in the text and with $C_{inter} = C_m$.

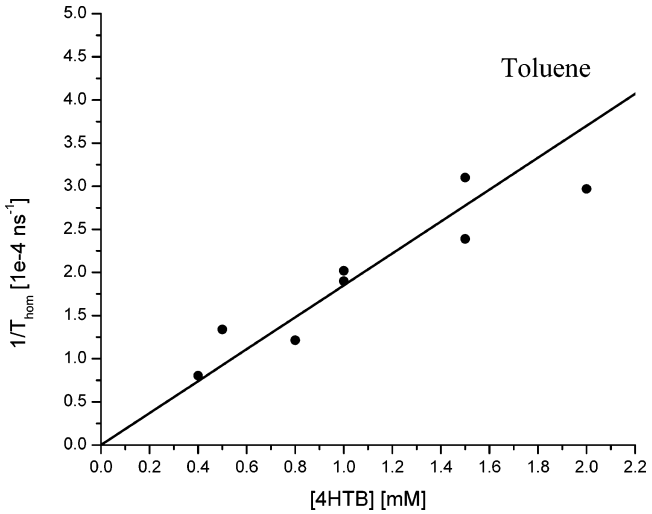

Figure 4. Exponential decay rate constant ($1/T_{hom}$) of the DEER decays vs [4HTB] for a toluene solution.

r_{max} value used, the simulations show that the plateau is reached between 6 and 10 μs whereas experimental results could be acquired only up to 1.5−2 μs. Hence, the data analysis must proceed via a fitting procedure using the full expression as given in eqs 10, 11, and 13. For example, the decay of 1 mM 4HTB in 7.5 wt % F127 micellar solution shown in Figure 3 was fitted with $r_{max} = 8.0$ nm, $M_{av} = 8.8$, and $C_{inter} = 0.1$ mM ($\chi = 10$).

The fitting process provides two essential parameters, M_{av} and r_{max}, which for spherical micelles is the diameter of volume occupied by 4HTB within the micelle. However, χ is another

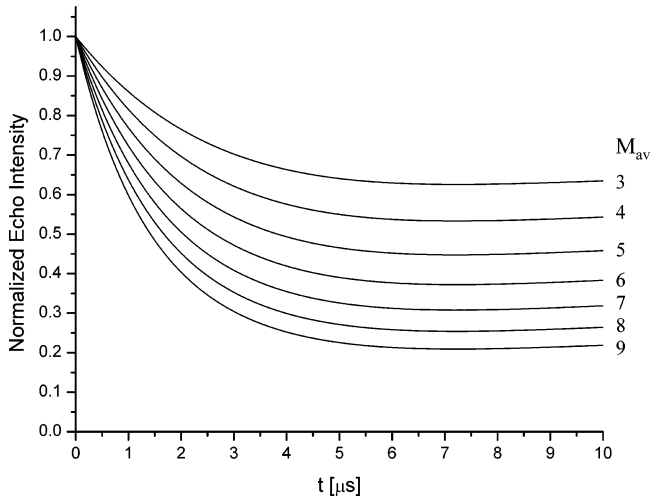

Figure 5. $V_{intra}(t)$ for various average number of spins (M_{av}) obtained using eq 13 and $r_{min} = 0.3$ nm, $r_{max} = 10$ nm, and $\lambda = 0.18$.

parameter that affects the decay, and we do not know it a priori. Accordingly, we carried out data fitting simulations for two limiting cases of χ. In the first, we took $\chi = M_{av}$, which corresponds to a single effective spin per micelle, such that $C_{inter} = [4HTB]/M_{av} = C_m$ and C_m is the concentration of micelles. In the second limit, $\chi = 1$ and $C_{inter} = [4HTB] = C_m M_{av}$.

To ensure that the curve fitting provides a unique value for M_{av}, r_{max}, and C_m, a series of measurements were carried out on samples with the same Pluronic concentration but different 4HTB concentrations. Such samples should have the same C_m. The aggregation number can be calculated from $N_{agg} = C_p/C_m$, where C_p is the Pluronic concentration. In practice, the fitting was done on 2−3 DEER decays simultaneously under the constraints that $M_{av1}/M_{av2} = [4HTB]_1/[4HTB]_2$. A plot of M_{av} vs [4HTB] yields a linear curve with an intercept at $M_{av} = [4HTB] = 0$ and a slope equal to C_m^{-1}. The parameters obtained are listed in Table 1, and the range corresponds to the values obtained using the two limits of χ. As expected, the range obtained was small showing that the contribution of $V_{inter}(t)$ is rather small and therefore the effect of χ is practically within the experimental error. Figure 6 shows the M_{av} dependence of 7.5 wt % F127 (black squares) and 6 wt % L64 solutions (open circles), and the parameters obtained are summarized in Table 1.

The volume of the hydrophobic core has been shown to be[13]

$$V_m = nV_{PO}N_{agg} \tag{18}$$

where n is the number of PO units in one Pluronic chain and $V_{PO} = 95.4$ Å^3 is the volume of one PO unit. Hence, using

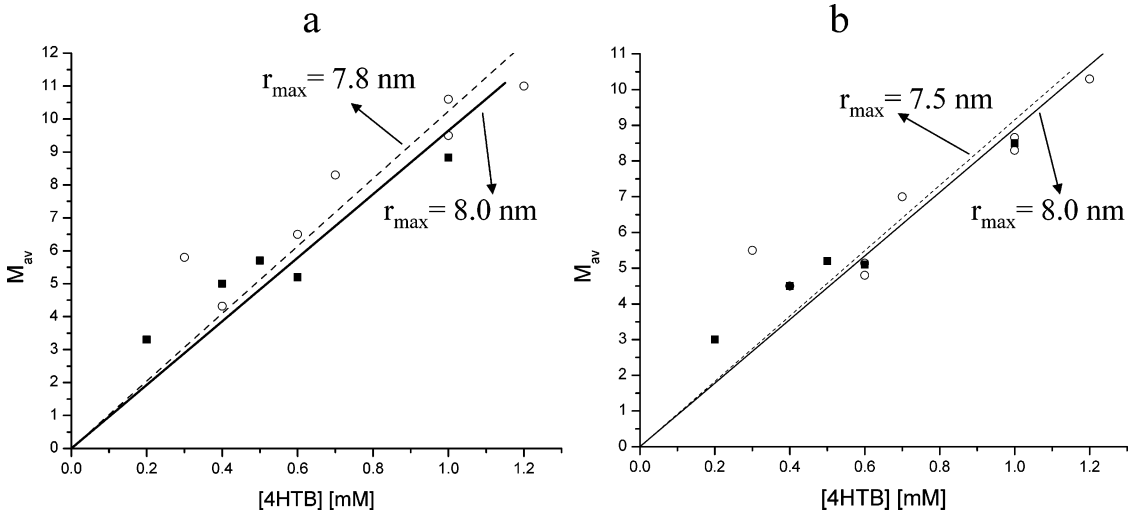

Figure 6. M_{av} vs [4HTB] for 7.5 wt % F127 (black square) and 6 wt % L64 (open circles), obtained with (a) $C_{inter} = C_m$ and (b) $C_{inter} = C_m M_{av}$.

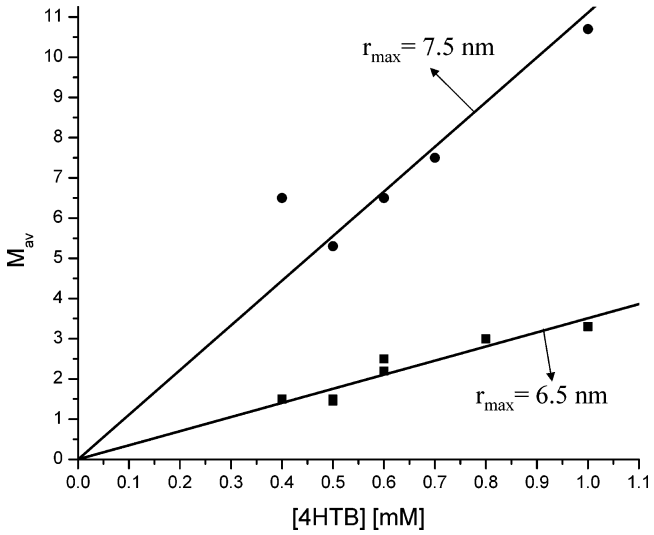

Figure 7. M_{av} vs [4HTB] for (i) 3 wt % F127, obtained with $C_{inter} = C_m M_{av}$ (squares), and (ii) 3 wt % P123 (circles), obtained with $C_{inter} = C_m$.

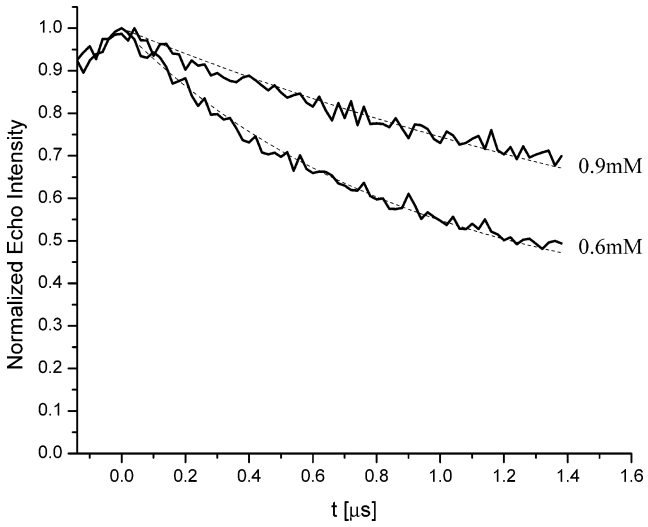

Figure 8. DEER signal of 0.9 mM and 0.6 mM 4HTB in 6 wt % P123. The dashed lines are best fit calculations, obtained with the parameters given in the text and with $C_{inter} = C_m$.

N_{agg} obtained from the DEER fitting, V_m was calculated and the diameter of the core of the micelle, d_c, was determined. The values of d_c listed in Table 1 show that 4HTB occupies a smaller volume than the full hydrophobic core ($r_{max} < d_c$). In 6 wt % L64, it occupies 74%, whereas in 7.5 wt % F127 it is distributed throughout 88−90% of the hydrophobic core. Hence, in F127 it can be found closer to the core−corona interface. This is consistent with the CW EPR results, where a larger coupling, a_N, was observed for 4HTB in 7.5 wt % F127. The C_m value for 6 wt % L64 and 7.5 wt % F127 was found to be around 0.1 mM, while N_{agg} is significantly larger in L64 (192−220 vs 55−59).

The dependence of M_{av} on [4HTB] for 3 wt % F127 is shown in Figure 7. In this solution, 4HTB is distributed between unimers and micelles (see CW EPR results) and, therefore, the limit $C_{inter} = C_m$ is irrelevant. Thus, here, calculations were carried out only for the upper value of C_{inter}, which is the total spin concentration. In this case, the plot of M_{av} vs [4HTB] yields a slope equal to $[C_m/(1 - P_{sl})]^{-1}$, where P_{sl} is the fraction of 4HTB located in the micelles. Taking $P_{sl} = 0.5$ as determined from the CW EPR spectrum yields $C_m = 0.142$ mM. In this case, $N_{agg} = C_p P_p / C_m$, where P_p is the fraction of the Pluronic molecules that are in micelles. Unfortunately, the EPR spectrum of F127−NO was not resolved enough to provide P_p, and therefore, we estimated it from the spectrum of P123−NO in F127 micelles, for which $P_p = 0.75$. The value obtained for N_{agg} after this assumption is 13. Since P123−NO is less hydrophilic than F127, its distribution between unimers and micelles may be different than that of F127. Moreover, we do not know if only one 4HTB molecule is solvated within the F127 monomers. Therefore, for this sample, N_{agg} is between 13 and 17 (corresponds to $P_p = 1$).

P123. The CW EPR spectrum of 4HTB in 3 wt % P123 showed that it is distributed between two environments of which one is more hydrophilic. The M_{av} dependence on [4HTB] is shown in Figure 7 for $C_{inter} = C_m$. For the two limiting cases of C_{inter} $N_{agg} = 52-60$ was obtained. The r_{max}/d_c ratio shows that 4HTB reaches areas closer to the core−corona interface than in 6 wt % L64 but farther than in 7.5 wt % F127 (see Table 1). While for 6 wt % L64, 7.5 wt % F127, and 3 wt % P123 the DEER decay rates exhibited a continuous behavior throughout the [4HTB] range studied, an unexpected decrease in the rate was observed in 6 wt % P123 for [4HTB] > 0.7 mM as shown in Figure 8. Analysis of the data assuming that the shape of the micelles is spherical (Figure 9) implied that this change is associated with a change from $r_{max} = 8.0$ nm and $N_{agg} = 114-128$ to $r_{max} = 12.5-12.8$ nm and $N_{agg} = 93-104$ (see Table 1). This change can be attributed to the swelling

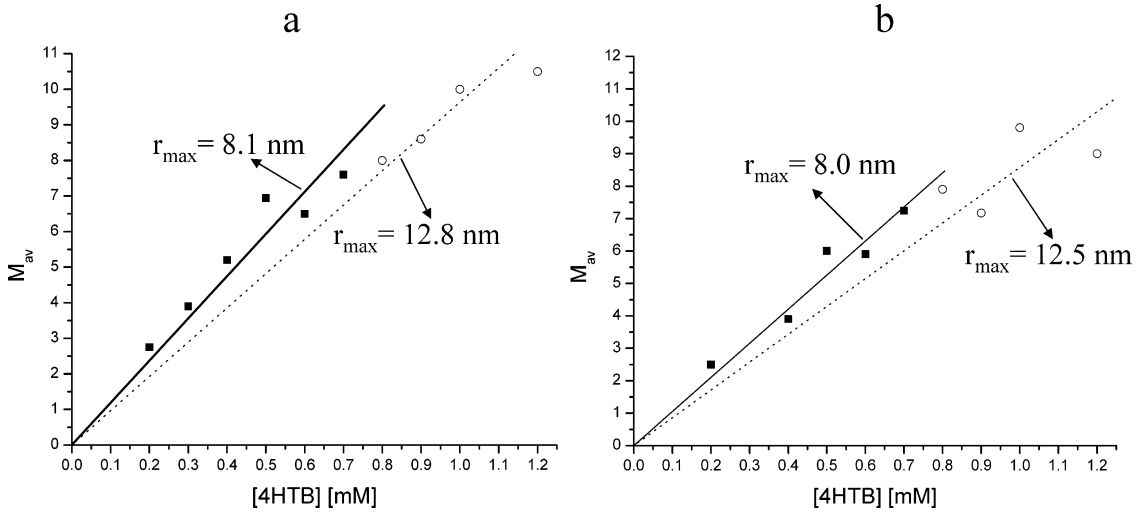

Figure 9. M_{av} as a function of [4HTB] for 6 wt % P123. The two lines correspond to the range [4HTB] ≤ 0.7 mM (squares, solid line) and [4HTB] > 0.7 mM (circles, dashed line). M_{av} was obtained from a model of spherical micelles and with (a) $C_{inter} = C_m$ and (b) $C_{inter} = C_m M_{av}$.

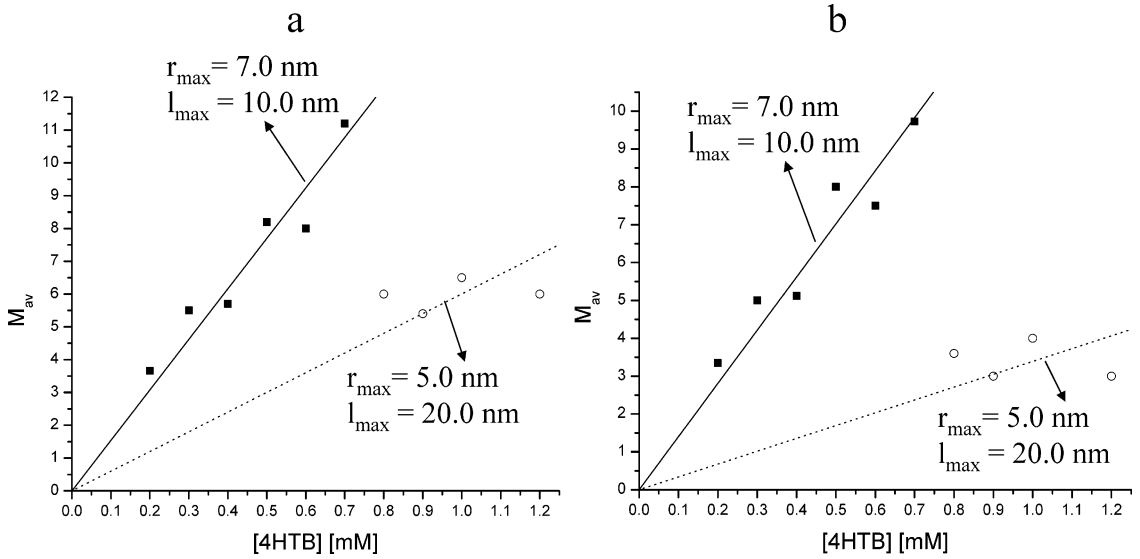

Figure 10. M_{av} as a function of [4HTB] for 6 wt % P123. The two lines correspond to the range [4HTB] ≤ 0.7 mM (squares, solid line) and [4HTB] > 0.7 mM (circles, dashed line). M_{av} was obtained from a model of rodlike micelles and with (a) $C_{inter} = C_m$ and (b) $C_{inter} = C_m M_{av}$.

of the hydrophobic core or to the migration of 4HTB into the corona region. The former possibility seems more likely because the change was not associated with an increase of a_N which would be expected in the case of migration.

While the micelles in 3 wt % P123 were reported to be spherical, there is some ambiguity regarding their shape at 6 wt % P123, because it was suggested that they may have a rod shape.[14,41] Hence, we analyzed the data also using a cylindrical model, given in eq 17. The fitted parameters were M_{av}, l_{max}, and r_{max} and C_m as described above. The results are shown in Figure 10. Up to [4HTB] = 0.7 mM, the DEER decays could be well simulated with $r_{max} = 7 \pm 0.1$ nm, $l_{max} = 10$ nm, and $N_{agg} = 159-165$. At [4HTB] > 0.7 mM, the best fit parameters were $r_{max} = 5 \pm 0.1$ nm, $l_{max} = 20$ nm, and $N_{agg} = 42-64$ (see Table 1). It is very unlikely that a small change in the spin-probe concentration would reduce N_{agg} by a factor greater than 2, without a phase transition. Hence, we conclude that the micelles at 6 wt % P123 cannot be rodlike at both high and low [4HTB] concentration ranges. Next, we considered the possibility that the discontinuity is due to a spherical → rodlike transition induced by the [4HTB]. This is also unlikely because it is associated with a decrease of N_{agg} from ∼120 to ∼50. However, a rodlike → spherical transition seems plausible, and it is associated with a decrease in N_{agg} from ∼160 to ∼100 along with an increase of C_m from ∼0.066 to ∼0.1 mM as would be expected from such a transition. Therefore, we find this possibility the most attractive and more likely than the swelling. This is also consistent with the discontinuity in the decay as expected for a phase transition.

Discussion

In this study, we have determined the size of the hydrophobic core of three types of block-copolymer micelles defined by the volume in which the hydrophobic spin-probe, 4HTB, is solubilized. To establish the methodology, we first compared the DEER decays of 6 wt % L64 and 7.5 wt % F127, the EPR spectra of which show that 4HTB is completely localized in the micelles and it senses only one type of environment. In addition, it is known from the literature that at the temperature and concentration used the micelles are spherical.[13] The radii obtained from the DEER measurements were 4.0 ± 0.05 and 3.8 ± 0.1 nm for the F127 and L64 micelles, respectively. The data analysis provided the aggregation number as well, which could be further used to calculate the volume of the hydrophobic core of the micelle, determined by the volume of the PPO

segments using the relation given in eq 18. N_{agg} was derived from C_m, which is obtained by fitting the experimental DEER decays. It was found that while in F127 88−90% of the core volume is occupied by 4HTB, in L64, it is only 74%.

Nagarajan[14] reported from SAXS and light-scattering measurements on 7 wt % Pluronic F127 micelles in water at 25 °C a hydrophobic core radius of 3.75 nm, a corona radius of 7.02 nm, and an aggregation value of 30. In this case, the volume was determined experimentally and N_{agg} was calculated from the Debye plots.[36] The value we obtained for 7.5 wt % F127 is 55−59, which is larger than 30. Nevertheless, our measurements were carried out on micelles freeze quenched from 50 °C and not at 25 °C, and therefore, the increase in aggregation number may be associated with the temperature difference, where N_{agg} increases with temperature according to $(T - T_{CMT})^{0.6}$.[13] The hydrodynamic radius of the micelles is, however, rather invariant to temperature changes because the corona becomes more compact and water is squeezed out from between the solvated EO groups, but the core radius increases with N_{agg}.[36,37] This is consistent with our results. Cryo-TEM measurements[38] reported hydrophobic core radii of 10.8 and 6 nm for 10 and 5 wt % F127, frozen from 50 °C, respectively, and SANS measurements gave a hydrophobic core radius of 5.0 nm for 5 wt % at 35 °C.[39] These values are somewhat larger than the core radius that we obtained (see Table 1). The DEER measurements carried out on 3 wt % F127 showed that they are sensitive to the distribution of the probe between unimers and micelles, but the combined EPR/DEER data were still insufficient to produce accurate r_{max} and N_{agg} values.

Several studies carried out on micellar solutions of L64 with a concentration below 8 wt % found the hydrodynamic radius to be between 6 and 8 nm, and at 40 °C, micelles with $N_{agg} = 35$ were reported.[1] Others reported that the core radius of spherical micelles in 8−32 wt % L64 solutions can vary between 3.4 and 4.6 nm and the N_{agg} value between 39 and 70 at 23−35 °C.[14] These N_{agg} values are, however, inconsistent with eq 18. Guo et al.[11] showed through SAXS measurements that the core radius in a 6 wt % L64 increases from 3.8 nm at 20 °C to 5.1 nm at 50 °C. While the 5.1−5.3 nm hydrophobic core radius we obtained for 6 wt % L64 at 50 °C is close to these values, N_{agg} is significantly larger (see Table 1) but consistent with eq 18.

The available data in the literature on P123 are more limited. Comparative dynamic and static light-scattering measurements on a P123 solution below 8 wt % at 25 °C gave a value of 9−9.6 nm for the hydrodynamic radius of the P123 micelle, 5 nm for the core radius, and an aggregation number of 100−120.[40] Flodström et al.[41] studied the formation of the mesoporous material SBA-15, synthesized with 3 wt % P123 aqueous solution by synchrotron SAXS. They reported that P123 micelles at 35 °C are spherical and 15 min after the addition of the silica source to the Pluronic aqueous solution, the radius of the micelles is 7 nm with a hydrophobic core radius close to 4.5 nm. Our measurements for 3 wt % P123 gave a core radius of 4.35−4.55 nm and an aggregation number of 52−60. More interesting were the results of the 6 wt % P123, which were found to be sensitive to the amount of 4HTB added and exhibited a phase transition at [4HTB] = 0.7 mM (this corresponds to a 15:1 P123/4HTB molar ratio). The most likely explanation of this transition is a rodlike-to-spherical transition. This implies that the addition of 4HTB swells the hydrophobic core and this translates further into the EO region, reducing its compactness and thereby leading to an increase in the curvature manifested in a phase transition to spherical micelles. The observation of the discontinuity in the DEER decay rates as a function of [4HTB] allowed us to assign the shape of the micelles at low 4HTB concentrations to rod-shaped micelles, the aspect ratio of which is rather low (see Table 1). These results show that DEER measurements are sensitive to variations in the shape/size of the aggregate and therefore may be applied to studies where such changes are of interest as in the formation process of mesoporous materials.

Finally, the agreement between the micellar sizes obtained from the DEER data and those reported in the literature and the fact that the results are consistent with the properties of the different Pluronics used in this study provide unambiguous evidence that the rapid freezing procedure used in this work preserves the micellar structure in the frozen solutions. Although a number of earlier experiments have shown that the micelles are preserved upon rapid freezing,[42,43] the results presented in this work comprise a significant addition. This turns the DEER method into a versatile technique in the sense that carefully chosen spin-probes, with tailored properties, can be used to probe different compartments of the micelles. In this work, which was designed to test the feasibility of the method, we chose the simplest case, a hydrophobic spin-probe which probes the hydrophobic core of the micelles. Alternatively, one can use more hydrophilic probes that will probe the size of the corona under various conditions. A disadvantage of the method is the time needed to acquire the data, which ranges from 3 h for one data point at relative high concentration (1 mM) to 12 h at low concentration (0.2 mM).

Conclusions

A methodology for measuring the sizes of micelles and their aggregation number by DEER has been demonstrated. It was found that the volume occupied by the hydrophobic spin-probe 4HTB in 7.5 wt % F127 and 6 wt % L64 is 88−90% and 74%, respectively, of the total volume of the hydrophobic core. The values obtained are within the range of values reported in the literature. It was also shown that the DEER decay senses distribution of the spin-probe between unimers and micelles, and, more importantly, changes in the shape of the micelles such as the detection of a transition from rodlike to spherical micelles. Finally, this study has shown unambiguously that micelles are preserved upon rapid freezing.

Note Added in Proof. Equation 13 implies a "stepwise" distribution function for the radicals over the sphere. Another relevant distribution function is a uniform distribution of radicals in the sphere. However, the fit of the experimental DEER decays with the latter (carried out using Monte-Carlo simulations) was substantially less satisfactory than with the former. This may suggest that the 4HTB distribution is inhomogeneous, with less spin-probes in the center of the core of the micelle.

Acknowledgment. This research was supported by the Center of Excellence, "Origin of Ordering and Functionality in Mesostructured Hybrid Materials", supported by the Israel Science Foundation (under Grant No. 800301-1), the Binational USA-Israel Science Foundation (BSF, Grant 2002175), and by a grant from the Ministry of Science, Israel awarded to S.R. The kind support of the Isle Katz Institute for Material Science and Magnetic Resonance Research is acknowledged.

References and Notes

(1) Booth, C.; Attwood, D. *Macromol. Rapid Commun.* **2000**, *21*, 501−527.

(2) Alexandridis, P.; Hatton, T. A. *Colloids Surf., A* **1995**, *96*, 1−46.

(3) Zhao, D.; Huo, Q.; Feng, J.; Chmelka, B. F.; Stucky, G. D. *J. Am. Chem. Soc.* **1998**, *120*, 6024−6036.
(4) Zhao, D.; Feng, J.; Huo, Q.; Melosh, N.; Fredrickson, G.; Chmelka, B. F.; Stucky, G. D. *Science* **1998**, *279*, 548−552.
(5) Van de Voort, P.; Benjelloun, M.; Vansant, E. F. *J. Phys. Chem. B* **2002**, *106*, 9027−9032.
(6) Su, Y. I.; Wang, J.; Liu, H. Z. *Macromolecules* **2002**, *35*, 6426−6431.
(7) Bryskhe, K.; Jansson, J.; Topgaard, D.; Schillen, K.; Olsson, U. *J. Phys. Chem. B* **2004**, *108*, 9710−9719.
(8) Wanka, G.; Hoffmann, H.; Ulbricht, W. *Macromolecules* **1994**, *27*, 4145−4159.
(9) Alexandridis, P.; Zhou, D.; Khan, A. *Langmuir* **1996**, *12*, 2690−2700.
(10) Bohorquez, M.; Koch, C.; Trygstad, T.; Pandit, N. *J. Colloid Interface Sci.* **1999**, *216*, 34−40.
(11) Guo, L.; Colby, R. H.; Lin, M. Y.; Dado, G. P. *J. Rheol.* **2001**, *45*, 1223−1243.
(12) Vasilescu, M.; Caragheorgheopol, A.; Caldararu, H. *Adv. Colloid Interface Sci.* **2001**, *89*−*90*, 169−194.
(13) Mortensen, K. *J. Phys.: Condens. Matter* **1996**, *8*, A103−A124.
(14) Nagarajan, R. *Colloids Surf., B* **1999**, *16*, 55−72.
(15) Zhou, L.; Schlick, S. *Polymer* **2000**, *41*, 4679−4689.
(16) Malka, K.; Schlick, S. *Macromolecules* **1997**, *30*, 456−465.
(17) Vasilescu, M.; Caragheorgheopol, A.; Caldararu, H.; Bandula, R.; Lemmetyinen, H.; Joela, H. *J. Phys. Chem. B* **1998**, *102*, 7740−7751.
(18) Caragheorgheopol, A.; Caldararu, H.; Vasilescu, M.; Khan, A.; Angelescu, D.; Žilková, N.; Čejka, J. *J. Phys. Chem. B* **2004**, *108*, 7735−7743.
(19) Caldararu, H. *Spectrochim. Acta, Part A* **1998**, *54*, 2309−2336.
(20) Jeschke, G.; Panek, G.; Godt, A.; Bender, A.; Paulsen, H. *Appl. Magn. Reson.* **2004**, *26*, 223−244.
(21) Milov, A. D.; Maryasov, A. G.; Tsvetkov, Yu. D.; Raap, J. *Chem. Phys. Lett.* **1999**, *303*, 135−143.
(22) Milov, A. D.; Tsvetkov, Yu. D.; Formaggio, F.; Crisma, M.; Toniolo, C.; Raap, J. *J. Am. Chem. Soc.* **2001**, *123*, 3784−3789.
(23) Milov, A. D.; Tsvetkov, Yu. D.; Formaggio, F.; Oancea, S.; Toniolo, C.; Raap, J. *J. Phys. Chem. B* **2003**, *107*, 13719−13727.
(24) Pannier, M.; Schöps, M.; Schädler, V.; Wiesner, U.; Jeschke, G.; Spiess, H. W. *Macromolecules* **2001**, *34*, 5555−5560.
(25) Pannier, M.; Veit, S.; Godt, A.; Jeschke, G.; Spiess, H. W. *J. Magn. Reson.* **2000**, *142*, 331−340.
(26) Caragheorgheopol, A.; Caldararu, H.; Dragutan, I.; Joela, H.; Brown, W. *Langmuir* **1997**, *13*, 6912−6921.
(27) Vandermeulen, G. W. M.; Hinderberger, D.; Xu, H.; Sheiko, S. S.; Jeschke, G.; Klok, H.-A. *ChemPhysChem* **2004**, *5*, 488−494.
(28) Salikhov, K. M.; Dzuba, S. A.; Raitsimring, A. M. *J. Magn. Reson.* **1981**, *42*, 255−276.
(29) Raitsimring, A. M.; Salikhov, K. M.; Umanskii, B. A.; Tsvetkov, Yu. D. *Sov. Phys. Solid. State* **1974**, *16*, 492−497.
(30) Raitsimring, A. M.; Salikhov, K. M. *Bull. Magn. Reson.* **1985**, *7*, 184−217.
(31) Milov, A. D.; Tsvetkov, Yu. D. *Appl. Magn. Reson.* **1997**, *12*, 495−504.
(32) Milov, A. D.; Maryasov, A. G.; Tsvetkov, Yu. D. *Appl. Magn. Reson.* **1998**, *15*, 107−143.
(33) Milov, A. D.; Ponomarev, A. B.; Tsvetkov, Yu. D. *Chem. Phys. Lett.* **1984**, *110*, 67−72.
(34) Ruthstein, S.; Frydman, V.; Kababya, S.; Landau, M.; Goldfarb, D. *J. Phys. Chem. B* **2003**, *107*, 1739−1748.
(35) Ruthstein, S.; Frydman, V.; Goldfarb, D. *J. Phys. Chem. B* **2004**, *108*, 9016−9022.
(36) Wanka, G.; Hoffman, H.; Ulbricht, W. *Colliod Polym. Sci.* **1990**, *268*, 101−117.
(37) Zhou, Z.; Chu, B. *J. Colloid Interface Sci.* **1988**, *126*, 171−180.
(38) Lam, Y.-M.; Grigorieff, N.; Goldbeck-Wood, G. *PCCP* **1999**, *1*, 3331−3334.
(39) Mortensen, K.; Talmon, Y. *Macromolecules* **1995**, *28*, 8829−8834.
(40) Nolan, S. L.; Phillips, R. J.; Cotts, P. M.; Dungan, S. R. *J. Colloid Interface Sci.* **1997**, *191*, 291−302.
(41) Flodström, K.; Teixeira, C. V.; Amenitsch, H.; Alfredsson, V.; Lindén, M. *Langmuir* **2004**, *20*, 4885−4891.
(42) Ottaviani, M. F.; Daddi, R.; Brustolon, M.; Turro, N. J.; Tomalia, D. A. *Langmuir* **1999**, *15*, 1973−1980.
(43) Zhang, J.; Carl, P. J.; Zimmermann, H.; Goldfarb, D. *J. Phys. Chem. B* **2002**, *106*, 5382−5389.